

Intrabeam Scattering

Andrzej Wolski

University of Liverpool, and the Cockcroft Institute, UK

Abstract

Intrabeam scattering refers to the effects of the Coulomb interaction acting between pairs of charged particles within a bunch in an accelerator. One of the main consequences of intrabeam scattering is a change in the emittances of a bunch: in some circumstances (in particular, in hadron storage rings operating above transition), the transverse and longitudinal emittances may grow over time without limit. This may restrict the performance of machines for which maintaining low beam emittance is an important requirement. In this note, we describe some of the models used to analyse the effects of intrabeam scattering, and present in particular the Piwinski formulae for the emittance growth rates. We compare the predicted changes in emittance with measurements in a number of machines operating in different parameter regimes.

Keywords

Intrabeam scattering; emittance growth; intensity limitations.

1 Introduction

As a bunch of charged particles moves along an accelerator beamline, particles interact through the Coulomb force. In principle, there are two ways in which the effects of the Coulomb interaction may be modelled: either, a bunch may be represented as a continuous charge distribution with a size and shape that evolve as the bunch moves along a beamline; or a bunch may be represented as a collection of discrete particles that scatter (or ‘collide’ with each other). The continuum model leads to the theory of space-charge [1, 2]; the discrete particle model leads to the effects of Touschek scattering [3] and intrabeam scattering [4, 5].

Touschek scattering and intrabeam scattering both involve transfer of energy and momentum between the (transverse and longitudinal) degrees of freedom. In Touschek scattering, however, the change in longitudinal momentum in a collision between two particles is large: in a storage ring, the change may be large enough that the final longitudinal momentum of one or both particles lies outside the acceptance of the ring, so that particles can be lost from the beam. ‘Large angle’ scattering events leading to particle loss are infrequent compared to the rate of ‘small angle’ scattering events; nevertheless, the steady loss of particles through Touschek scattering (quantified by the Touschek lifetime) is often a dominant limitation on the lifetime of beams in low-emittance electron storage rings.

The frequent collisions leading to smaller changes in momentum (intrabeam scattering, IBS) also have observable effects: although particles are not lost from the beam, there can be significant changes in beam emittance. The changes that occur depend on whether the storage ring is operating below or above transition. As we shall see in Section 3.1, below transition a simple model may be developed in which the particles in a bunch behave as atoms or molecules in an ideal gas. Scattering then leads to the particles reaching an equilibrium distribution, with the energy shared between the different degrees of freedom. Above transition, however, the behaviour is very different: in that case, there is no equilibrium, but the emittances can grow without limit.

The timescale of changes in beam emittance from intrabeam scattering depends on many factors, including the beam energy, the charge density within the bunch and the storage ring optics. Over a wide range of parameter regimes, emittance growth times are on the timescale of minutes or hours. For hadron

colliders, this can limit the luminosity lifetime and require the injection of fresh (low-emittance) bunches of particles at regular intervals. In electron storage rings, synchrotron radiation damping generally dominates over emittance growth from intrabeam scattering (though particle loss from Touschek scattering is often an important limitation on beam lifetime). However, for the latest generation of ultra-low emittance electron storage rings for synchrotron light sources, the particle density can be high enough that intrabeam scattering leads to an increase of the equilibrium emittance that would be achieved through synchrotron radiation effects acting alone. Intrabeam scattering has even been observed in a high-brightness driver for a free-electron laser [6].

The main goal of theoretical analysis of intrabeam scattering is to determine formulae for the emittance growth rates. Some early analysis was done in the late 1960's, but more thorough investigations were carried out in the early 1970's initially motivated by the realisation that intrabeam scattering could limit the luminosity of collisions in the SPS at CERN. The first detailed expressions for the emittance growth rates resulting from intrabeam scattering were derived (with some simplifications) by Anton Piwinski in 1974 [4]. Calculation of the growth rates using Piwinski's formulae in a given machine can be computationally expensive, primarily because the growth rates are expressed in terms of integrals that must be evaluated numerically. The integrals depend on the lattice functions, so an accurate calculation of the growth rates requires a numerical integration to be performed at many individual points around the lattice. Soon after Piwinski's work, an alternative formulation of the intrabeam scattering growth rates was developed by Bjorken and Mtingwa [5]. Although the expressions for the growth rates in Bjorken and Mtingwa's formulae take a different form from those in Piwinski's formulae, they lead to the same results (and evaluation can still be computationally expensive). In the following years and decades, further work aimed to improve the accuracy of the formulae by including effects neglected in the original analysis and to simplify or approximate the expressions to allow faster computation. This has led to some more convenient ways to estimate the emittance growth rates from IBS in certain regimes, for example in high-energy storage rings.

Experimental studies of intrabeam scattering are often challenging because of the difficulty of separating different sources of emittance growth. For example, in hadron storage rings impedance effects and nonlinear effects can contribute to emittance growth on similar timescales to IBS. Nevertheless, studies have been carried out on several machines (including proton, ion and electron storage rings) covering a wide range of parameter regimes, with results that are generally consistent with the theories¹. Intrabeam scattering is now generally considered to be a well-understood phenomenon. The fundamental nature of the scattering process means that IBS is often a significant issue in storage rings requiring high-intensity, low emittance beams.

In the following sections, we first present some examples of observations of intrabeam scattering effects in different machines. We then discuss a simple model based on treating the particles within a bunch as atoms or molecules in an ideal gas: although this model is too basic to be of practical use in calculating growth rates, it does provide some insight into some significant features of IBS. It can help to explain, for example, why IBS leads to a beam reaching a new equilibrium distribution in a storage ring below transition whereas above transition the emittances can grow without limit. After discussing the simple 'ideal gas' model, we present Piwinski's formulae for the IBS emittance growth rates. We do not attempt to show a full derivation, as this is rather lengthy and mathematically involved: more complete treatments can readily be found in other places. We also discuss some of the significant theoretical developments aiming (for example) to provide simpler formulae for calculating the IBS growth rates in particular regimes. Finally, we present some examples of experimental measurements aiming to compare the growth rates from IBS in real machines with the predictions of the theoretical formulae.

¹It is often necessary to make some assumptions for certain beam parameters when comparing experimental results with theories of IBS, since it is not always possible to make direct measurements of all the quantities needed for the theoretical calculations.

2 Some observations of intrabeam scattering

Before discussing theoretical models and IBS growth rate formulae, we show some examples of the effects of intrabeam scattering. For our examples, we have selected three very different machines: two proton storage rings, one operating at 270 GeV (the CERN SPS [7]) and the other at 400 MeV (CELSIUS at The Svedberg Laboratory, Uppsala, Sweden [8]), and an electron storage ring (CESR at Cornell University, Ithaca, New York, USA [9]). Some of the relevant parameters for these accelerators are listed in Table 1. Further examples, showing more detailed comparisons between measurements and theoretical predictions, will be given in Section 4.

Some of the earliest detailed observations of intrabeam scattering effects were made in the CERN SPS in the early 1980's. An example of the measurements is shown in Fig. 1 [7] (see also Fig. 2 in Ref. [5]). The left-hand plot shows measurements of the longitudinal profile of a bunch of protons (left) and antiprotons (right) made at intervals of 30 minutes. An increase in bunch length can be seen in both cases, but is more evident for the proton bunch because of the relatively high population of the proton bunch (of order 10^{11} particles, compared to order 10^{10} particles for the antiproton bunch). The central plot shows the longitudinal emittance measured at intervals over a period of 8 hours, for three proton bunches with different bunch populations. The experimental measurements (data points) are compared with theoretical predictions (lines). The right-hand plot shows corresponding measurements of the horizontal emittance.

The measurements show good agreement between measurements and theoretical predictions. It is worth noting that other possible sources of emittance growth were excluded: growth rates from gas scattering, for example, were estimated to be an order of magnitude lower than those observed in the machine under the given conditions. It can also be seen in Fig. 1 that the growth rates fall off as the bunch emittance increases: this is expected for IBS, where the scattering rates are reduced for lower particle density, but would not be expected for gas scattering.

Another example of emittance growth from intrabeam scattering is shown in Fig. 2. In this case, measurements of the horizontal beam size in a 400 MeV proton beam in CELSIUS are presented. The bunch population is similar to that shown in Fig. 1 for the SPS, but in CELSIUS there is a clear increase in the emittance on a timescale of seconds, rather than tens of minutes for the SPS. The reason for the much larger emittance growth rate in CELSIUS is the beam energy: whereas the SPS measurements were performed at 270 GeV, the CELSIUS measurements were made at 400 MeV. The growth rates also depend on the beam size and lattice functions, but the significant difference between the two cases here is the difference in beam energy.

As a final example, measurements of IBS emittance growth are shown (for a very different regime) in Fig. 3 for the Cornell electron storage ring, CESR. As already mentioned, in electron storage rings the emittance growth rates from IBS are generally much slower than the damping rates from synchrotron

Table 1: Representative beam parameters in storage rings chosen to illustrate observations of intrabeam scattering.

| | SPS [7] | CELSIUS [8] | | CESR [9] |
|------------------------|-------------------|---------------------|-----------|--|
| Particle type | proton/antiproton | protons | ions | electrons/positrons |
| Beam energy (max) | 270 GeV | 400 MeV | 200 MeV/u | 2.085 GeV |
| Bunch population | 10^{11} | 10^{11} | 10^{10} | $1.6 \times 10^9 - 1.6 \times 10^{11}$ |
| Bunch length | | not known | | 10 mm |
| Relative energy spread | | 10^{-4} (assumed) | | 8×10^{-4} |
| Longitudinal emittance | 1 eV s | | | |
| Transverse emittance | 20π mm mrad | 1π mm mrad | | $3.4 \text{ nm} \times 20 \text{ pm}$ (h \times v, geometric) |

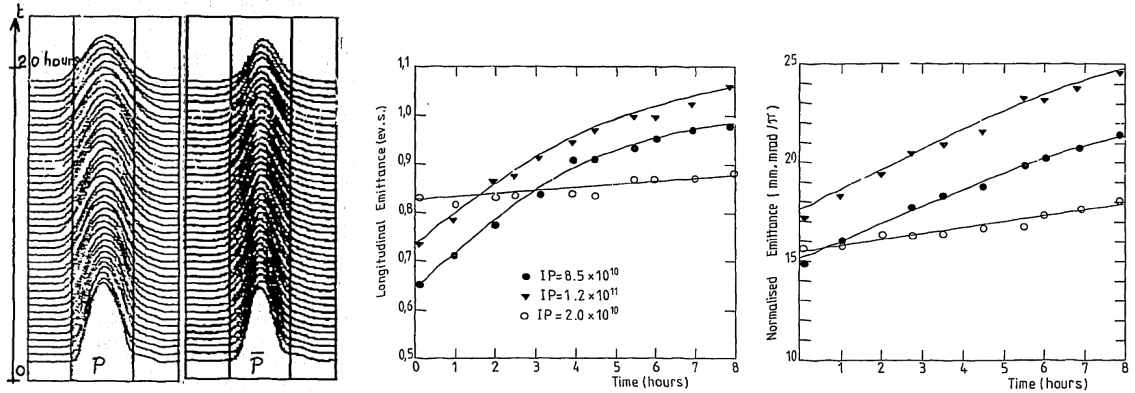


Fig. 1: Longitudinal and transverse emittance growth in the SPS [7]. The left-hand plot shows longitudinal charge density measurements of proton and antiproton bunches (left-hand and right-hand sides of the plot, respectively) made every 30 minutes, with successive measurements aligned from the bottom to the top of the plot. There is a larger increase in the bunch length for protons than antiprotons because of the larger bunch population (of order 10^{11} protons compared to 10^{10} antiprotons). The middle and right-hand plots show (respectively) the growth in longitudinal and transverse emittance over time for proton bunches with different bunch populations.

radiation. However, the very low vertical emittance that was achieved in CESR made it possible to observe an increase in the equilibrium emittances as a function of bunch charge: the equilibrium is determined by a balance between radiation damping, quantum excitation (again from synchrotron radiation) and intrabeam scattering. If the charge density in a bunch is high enough, then the IBS emittance growth rates may be fast enough to have an observable impact on the equilibrium emittance in an electron storage ring.

3 Theoretical models and growth-rate formulae

3.1 A simple gas model

As a first step towards a theoretical analysis of intrabeam scattering, we can consider a model in which the particles within a bunch in an accelerator are represented as atoms or molecules in an ideal gas. This is clearly a greatly simplified picture of the system: it is not sufficiently accurate to provide a basis for quantitative estimates of IBS growth rates, but it can give some insight into the very different effects of IBS in storage rings operating below and above transition.

Consider first the case of a hadron storage ring operating below transition. In most storage rings, higher energy particles follow a dispersive trajectory that generally has a larger circumference than the nominal trajectory for particles with the design energy. However, below transition the beam energy is low enough that the particle velocities are not ultra-relativistic: a higher energy particle then has a higher velocity that more than compensates the increase in the length of its trajectory over one turn around the storage ring. Hence, the revolution period of a particle *decreases* as the energy of the particle *increases*: this is illustrated in Fig. 4 (a).

In a storage ring below transition, particles scatter off each other in a way analogous to collisions between particles in an ideal gas. One important difference is that while the forces between particles in an ideal gas can be considered to be short-range (as long as the particles carry no net electric charge) the Coulomb force between charged particles in an accelerator acts over relatively long distances. A further difference is that an ideal gas is normally held in a container with rigid walls, and particles move freely within the container until they collide with a wall or with another particle. In the case of particles in an accelerator, we can represent the particles as moving within a potential well provided by the transverse

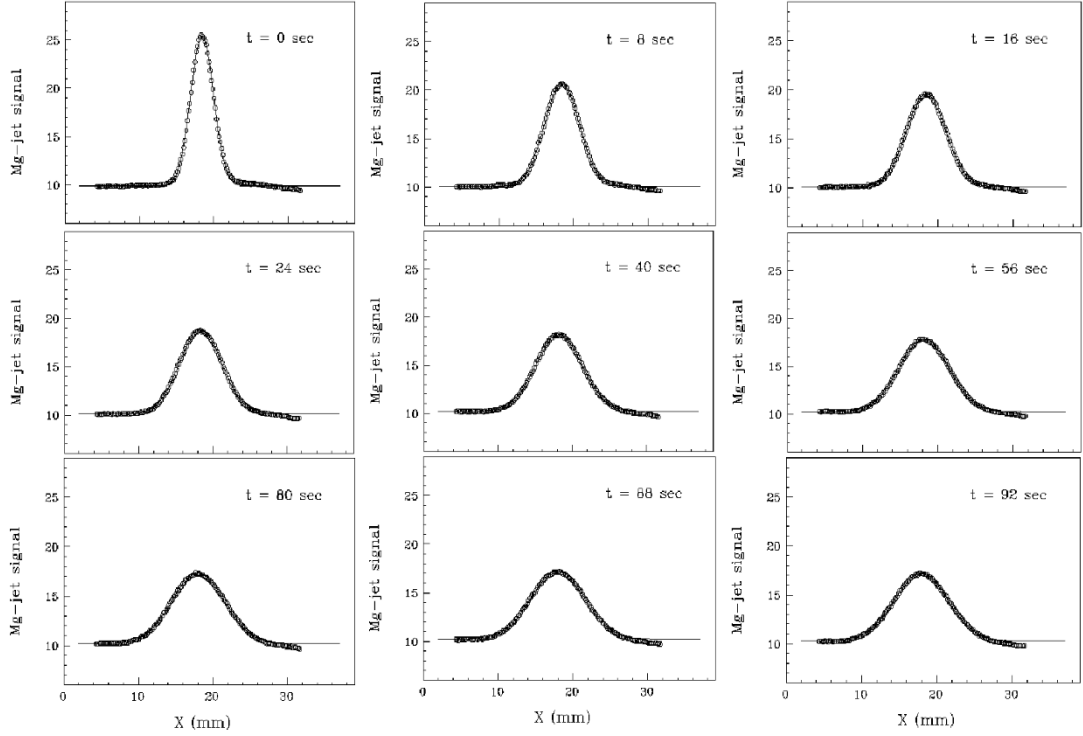


Fig. 2: Transverse emittance growth in CELSIUS [8]. Each plot shows the charge density in a 400 MeV proton bunch in the storage ring as a function of horizontal position within the bunch. The protons are first accumulated and then accelerated to 400 MeV with beam cooling turned on. For purposes of the measurements shown, the cooling is turned off after the bunch has reached equilibrium at 400 MeV, following which measurements are made at intervals for a total time of 92 seconds. Circles show measured data, and the lines show Gaussian fits.

and longitudinal focusing from the magnets and RF cavities in the storage ring lattice.

Putting these differences aside, the important process for intrabeam scattering, namely the transfer of momentum between the degrees of freedom through elastic collisions between pairs of particles, is essential similar in both cases. Let us further simplify the system by considering just longitudinal motion and transverse motion in one dimension (either horizontal or vertical). Assuming that the potential well from the longitudinal and transverse focusing forces is quadratic, the energy of a particle with mass m may be written (in the rest frame of the bunch, in a storage ring below transition):

$$E_{\text{particle}}^{(\text{below})} = \frac{1}{2}mv_x^2 + \frac{1}{2}k_x x^2 + \frac{1}{2}mv_z^2 + \frac{1}{2}k_z z^2, \quad (1)$$

where x and z are the horizontal and longitudinal coordinates (respectively) with corresponding velocities v_x and v_z , and the transverse and longitudinal focusing strengths are characterised by the constants k_x and k_z . Given this expression for the energy of a particle and the fact that particles exchange energy and momentum through elastic collisions, we can apply conservation of energy, so that:

$$m\langle v_x^2 \rangle + k_x \langle x^2 \rangle + m\langle v_z^2 \rangle + k_z \langle z^2 \rangle = \frac{2E_{\text{total}}}{N} = \text{constant}, \quad (2)$$

where the brackets $\langle \rangle$ indicate an average over all particles in the bunch, there are N particles in the bunch and the total particle energy (in the rest frame of the bunch) is E_{total} .

With some fairly general assumptions, we can derive relationships between the mean square coordinates $\langle x^2 \rangle$, $\langle z^2 \rangle$ and the mean square velocities $\langle v_x^2 \rangle$, $\langle v_z^2 \rangle$. For a single oscillator in one dimension, we

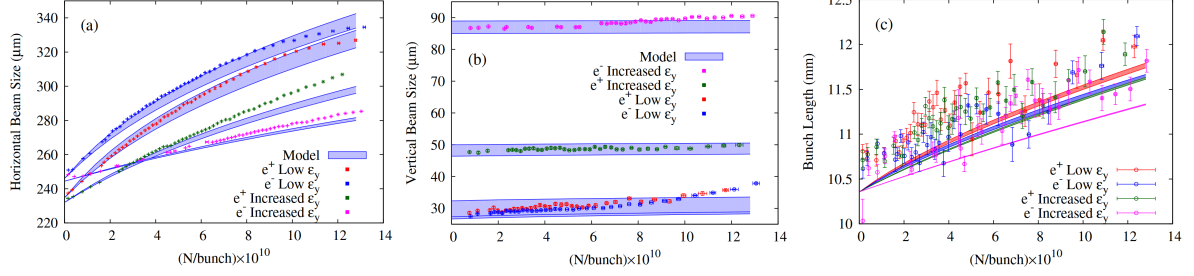


Fig. 3: Longitudinal and transverse emittance growth in the CESR storage ring [9]. Plots show the equilibrium horizontal (left) and vertical (middle) beam sizes and bunch length (right) as functions of bunch population for electron and positron bunches. Points show measurements and bands show theoretical predictions, taking into account uncertainties in the beam conditions. The vertical emittance can be controlled by adjusting the coupling using skew quadrupoles. Lower vertical emittances lead to larger equilibrium horizontal emittance and bunch length because of the effects of intrabeam scattering.

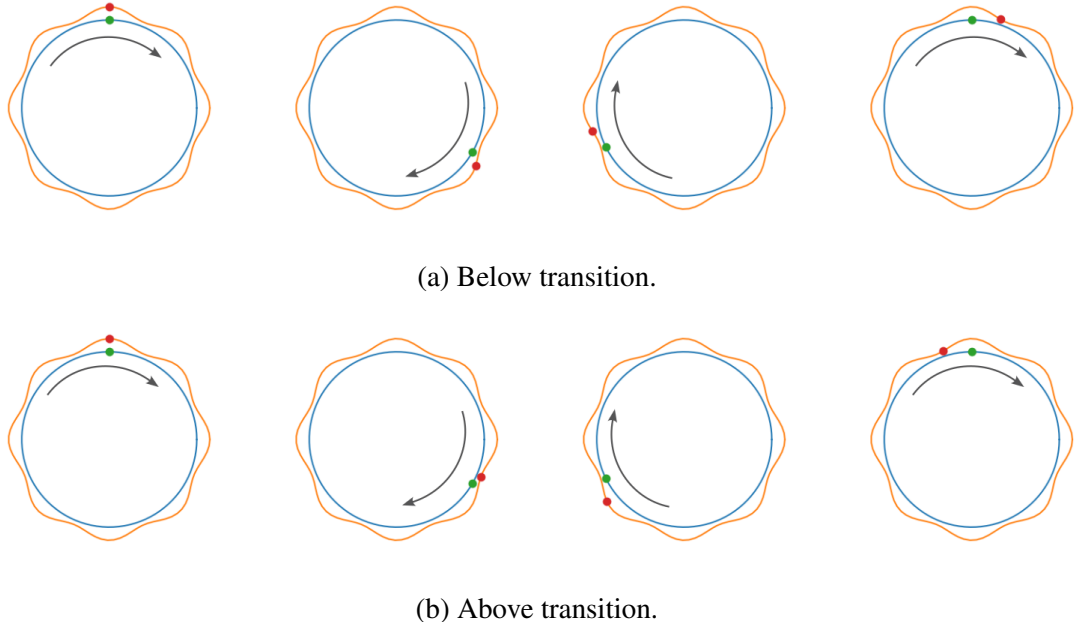


Fig. 4: Longitudinal motion of particles in a storage ring (a) below transition and (b) above transition. In both cases, a higher-energy particle (represented by the red dot on the orange outer path) follows a longer trajectory than a lower-energy particle (green dot on the blue inner path). Below transition, the higher velocity associated with higher energy more than compensates the increase in path length over one turn, so the revolution period falls with increasing energy. Above transition, particles are relativistic so that the increase in velocity with energy is negligible, and because of the larger path length, higher-energy particles take longer to complete each turn than lower-energy particles.

can write the equation of motion:

$$x = A \sin(\omega t + \psi), \quad (3)$$

where $\omega = \sqrt{k_x/m}$, and the amplitude A and initial phase ψ are constants. It follows that the averages

of x^2 and v_x^2 over a long time interval (i.e. long compared to the oscillation period) are:

$$\langle x^2 \rangle_t = \frac{1}{2} A^2, \quad \langle v_x^2 \rangle_t = \frac{1}{2} \omega^2 A^2, \quad (4)$$

and hence:

$$k_x \langle x^2 \rangle_t = m \langle v_x^2 \rangle_t. \quad (5)$$

Given a large collection of particles with random amplitudes and initial phase angles (so that each particle at any moment is at a different phase in its cycle of oscillation) we expect the same relationship to hold between the mean square coordinate and mean square velocity with the mean values now taken over all particles at a given time². Extending the argument to include (separately) the longitudinal motion, we then have:

$$m \langle v_x^2 \rangle = k_x \langle x^2 \rangle, \quad \text{and} \quad m \langle v_z^2 \rangle = k_z \langle z^2 \rangle. \quad (6)$$

In the context of accelerator beam dynamics, Eqs. (6) are the conditions for a *matched* distribution in a storage ring: the shape of the distribution of a bunch of particles in a storage ring will not change over time if the distribution is correctly matched to the focusing in the lattice. In terms of statistical mechanics, each of the equations in Eq. (6) is essentially a statement of equipartition of energy applied to a collection of particles in equilibrium for the transverse and longitudinal motion separately.

Assuming that the particle velocities are not correlated with the coordinates³ so that $\langle xv_x \rangle = \langle zv_z \rangle = 0$, the (geometric) emittances can be written:

$$\varepsilon_x = \frac{1}{P_0} \sqrt{\langle x^2 \rangle \langle p_x^2 \rangle}, \quad \varepsilon_z = \frac{1}{P_0} \sqrt{\langle z^2 \rangle \langle p_z^2 \rangle}, \quad (7)$$

where $p_x = mv_x$, $p_z = mv_z$, and P_0 is the reference momentum (the momentum of a particle with the design energy of the beam in the laboratory frame). Combining Eqs. (2), (6) and (7) we find:

$$P_0 \sqrt{\frac{k_x}{m}} \varepsilon_x + P_0 \sqrt{\frac{k_z}{m}} \varepsilon_z = \frac{E_{\text{total}}}{N} = \text{constant}. \quad (8)$$

Equation (8) must be satisfied even in the presence of any effect, such as intrabeam scattering, that can cause an exchange of energy between the transverse and longitudinal motion. An increase in energy in the transverse direction will increase the transverse emittance ε_x : but then we see that the longitudinal emittance ε_z must be reduced. Starting from a distribution with arbitrary transverse and longitudinal emittances, the bunch will move towards an equilibrium in which equipartition of energy is satisfied even taking into account the exchange in energy and momentum between the transverse and longitudinal motion:

$$m \langle v_x^2 \rangle = k_x \langle x^2 \rangle = m \langle v_z^2 \rangle = k_z \langle z^2 \rangle. \quad (9)$$

The above arguments are readily extended to three degrees of freedom. In a storage ring below transition, conservation of energy means that although IBS causes a transfer of energy and emittance between the degrees of freedom, the emittances will always satisfy:

$$\sqrt{k_x} \varepsilon_x + \sqrt{k_y} \varepsilon_y + \sqrt{k_z} \varepsilon_z = \text{constant}. \quad (10)$$

Below transition, the beam will reach an equilibrium in which the emittances satisfy the equipartition of energy:

$$\sqrt{k_x} \varepsilon_x = \sqrt{k_y} \varepsilon_y = \sqrt{k_z} \varepsilon_z. \quad (11)$$

²The fact that we can substitute averages over all particles for averages over time in equation (5) follows from the ergodic theorem.

³Since $\langle xp_x \rangle = -\alpha_x \varepsilon_x$, where p_x is the particle momentum (in the laboratory frame), $\alpha_x = -\frac{1}{2} d\beta_x/ds$ is the Twiss alpha function (related to the derivative of the beta function β_x), assuming that $\langle xv_x \rangle = 0$ implies that $\alpha_x = 0$ and hence $\beta_x = \text{constant}$.

In a storage ring above transition, the situation is very different. In this regime, particles now have ultra-relativistic velocities in the laboratory frame. A particle with energy above the reference energy will again follow a dispersive trajectory with a circumference that is longer than the nominal trajectory; but because the particle is ultra-relativistic there is negligible difference in the velocity compared to the velocity of a particle with the reference energy. As a result, the orbital period for a particle will *increase* with an increase in energy: see Fig. 4 (b). In the rest frame of the bunch, this is as if an increase in the longitudinal velocity was associated with a *reduction* in energy. In the transverse directions there is no change compared to the case of a storage ring below transition: an increase in velocity in a transverse direction will still be associated with an increase in energy.

Despite the change in the nature of the longitudinal motion, we can still apply the ideal gas model to understand the properties of the bunch, as long as we treat particles as having *negative mass* for their longitudinal motion: a force acting in the $+z$ direction will lead to a change in velocity towards the $-z$ direction. This implies that to maintain a bunched beam, the focusing in the longitudinal direction must also now be negative ($k_z < 0$). This is of course the situation in a real storage ring: below transition, the RF cavities must be phased so that bunches cross the cavities on a rising slope of the voltage (particles with higher energy with lower revolution period arrive earlier at a cavity and see a lower RF voltage); but above transition, the cavities must be phased so that bunches cross the cavities on a falling slope of the RF voltage. In terms of the potential energy of particles (viewed in the rest frame of the bunch), the larger the longitudinal co-ordinate z , the more negative the potential energy of the particle.

Taking these differences into account, for a storage ring above transition the expression corresponding to Eq. (1) for the energy of a particle is:

$$E_{\text{particle}}^{(\text{above})} = \frac{1}{2}mv_x^2 + \frac{1}{2}k_x x^2 - \frac{1}{2}|m|v_z^2 - \frac{1}{2}|k_z|z^2. \quad (12)$$

Equation (6) for the shape of the distribution treating each degree of freedom independently is still valid; and we can still use the definitions Eq. (7) for the emittances. But a larger longitudinal emittance corresponds to a more negative (i.e. lower) energy, and then following the same reasoning as for the case of a storage ring below transition, conservation of energy now leads to:

$$\sqrt{k_x}\varepsilon_x + \sqrt{k_y}\varepsilon_y - \sqrt{|k_z|}\varepsilon_z = \text{constant}. \quad (13)$$

The minus sign before the final term on the left hand side of this equation has a significant consequence: *below* transition conservation of energy required at least one emittance to shrink in order for another emittance to grow, but *above* transition all three emittances can grow indefinitely. In a storage ring operating above transition, there is no beam equilibrium (i.e. there is no condition that would correspond to Eq. (11) in the case of a storage ring below transition).

Of course, intrabeam scattering simply provides a means for exchange of momentum of particles between the different degrees of freedom, and the simple gas model we have used in the above arguments cannot provide a fully detailed description of the effects of IBS. The model does offer some insight into the very different impact of IBS in a storage ring above transition compared to the case of a storage ring below transition; but to make any precise predictions of IBS effects in either case, the details of the scattering process must be considered.

3.2 Piwinski formulae for IBS growth rates

The fundamental process that takes place when two particles within a single bunch in a hadron accelerator collide with each other is Rutherford scattering. Formulae for the rates of change of the bunch emittances as a result of the scattering process can be derived starting from a formula for the rate of scattering of particles from one region of momentum space to another. This depends on the phase space density of particles (the number of particles per unit volume of co-ordinate space and momentum space), the energies of the particles, and the scattering amplitude. The scattering amplitude describes the interaction between particles at the quantum level.

Consider a collection of particles in a small volume of co-ordinate space d^3x . Particles within this volume will have a range of momenta. In the laboratory frame, the rate of scattering of pairs of particles from regions of momentum space d^3p_1, d^3p_2 (for the two members of the pair) to regions $d^3p'_1, d^3p'_2$ can be written:

$$\begin{aligned} \frac{d\mathcal{P}}{dt} = & \frac{1}{2} \rho(x, p_1) \rho(x, p_2) d^3x \frac{d^3p_1}{\gamma_1} \frac{d^3p_2}{\gamma_2} \cdot |\mathcal{M}|^2 \cdot \frac{d^3p'_1}{\gamma'_1} \frac{d^3p'_2}{\gamma'_2} \\ & \times \frac{\delta^{(3)}(p'_1 + p'_2 - p_1 - p_2) \delta(E'_1 + E'_2 - E_1 - E_2)}{(2\pi)^2}, \end{aligned} \quad (14)$$

where $\rho(x, p)$ is the phase space density of the beam, and \mathcal{M} is the scattering amplitude. Note that this formula for the scattering rate is given in the laboratory frame where the two particles involved in the scattering process have energies E_1 and E_2 . For protons, the scattering amplitude \mathcal{M} is given by:

$$\mathcal{M} = \frac{4\pi\alpha}{q^2}, \quad (15)$$

where $\alpha \approx 1/137$ is the fine structure constant, and q is the change in four-momentum of either particle during the collision. The rate of change of the mean value $\langle g \rangle_{\text{PS}}$ of any function $g(x, p)$ of the phase space variables is given by:

$$\frac{d}{dt} \langle g \rangle_{\text{PS}} = \int_{\text{PS}} \frac{d\mathcal{P}}{dt} (g(x, p'_1) - g(x, p_1) + g(x, p'_2) - g(x, p_2)), \quad (16)$$

where the brackets $\langle \cdot \rangle_{\text{PS}}$ indicate an average over phase space, and the integral is taken over all phase space.

Equations (14), (15), and (16) provide the basic formulae needed to calculate the rate of change of emittance of a bunch in an accelerator as a result of IBS. The calculation is not straightforward, however, because of the nature of the integrals involved even for “simple” Gaussian beams. Furthermore, the phase space distribution of a bunch will change according to the variation of the lattice functions as the bunch moves along an accelerator beam line. This means that in a storage ring, further integrals must be performed to average the growth rates around the circumference of the ring. Depending on the details of how the calculation is performed, including any assumptions or approximations (e.g. assuming constant values for the beta functions) different expressions can be obtained for the growth rate formulae.

The earliest complete analysis of the IBS growth rates was performed by Piwinski [4]. Piwinski’s original calculation assumed a Gaussian beam distribution and neglected beta function gradients (which lead to correlations between co-ordinates and momenta in phase space). The calculations yield formulae for the IBS growth rates $1/\tau_i$, defined by⁴:

$$\frac{d\varepsilon_i}{dt} = \frac{2\varepsilon_i}{\tau_i}, \quad (17)$$

where $i = x, y, z$ for the horizontal, vertical and longitudinal emittance and growth rate, respectively. In Piwinski’s theory, the formulae for the growth rates can be written:

$$\frac{1}{\tau_x} = A \left\langle f\left(\frac{1}{\tilde{a}}, \frac{\tilde{b}}{\tilde{a}}, \frac{\tilde{q}}{\tilde{a}}\right) + \frac{\eta_x^2 \sigma_h^2}{\beta_x \varepsilon_x} f(\tilde{a}, \tilde{b}, \tilde{q}) \right\rangle_C, \quad (18)$$

$$\frac{1}{\tau_y} = A \left\langle f\left(\frac{1}{\tilde{b}}, \frac{\tilde{a}}{\tilde{b}}, \frac{\tilde{q}}{\tilde{b}}\right) + \frac{\eta_y^2 \sigma_h^2}{\beta_y \varepsilon_y} f(\tilde{a}, \tilde{b}, \tilde{q}) \right\rangle_C, \quad (19)$$

⁴The factor of 2 on the right hand side of Eq. (17) is included by analogy with the conventional definition of the synchrotron radiation damping times in electron storage rings: since the beam size is proportional to the square root of the emittance, if the emittance damps with exponential time constant 2τ , then the beam size damps with time constant τ .

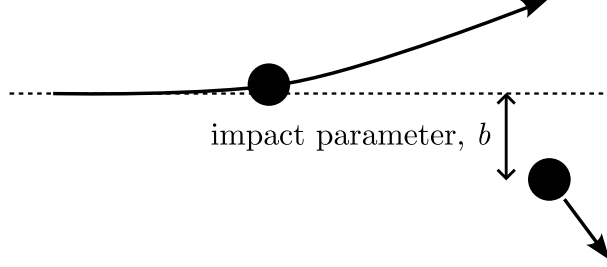


Fig. 5: In a collision between two particles, observed in a frame in which one particle is initially at rest, the impact parameter (b in the figure) measures the perpendicular distance between the initial trajectory of the moving particle and the initial position of the stationary particle.

$$\frac{1}{\tau_z} = A \left\langle \frac{\sigma_h^2}{\sigma_\delta^2} f(\tilde{a}, \tilde{b}, \tilde{q}) \right\rangle_C. \quad (20)$$

The brackets $\langle \cdot \rangle_C$ denote an average around the circumference of the ring. The factor A describes the scaling of the growth rates with energy and the phase space density, and is given by:

$$A = \frac{\pi r_0^2 c N_b}{8\gamma_0 \Gamma}, \quad (21)$$

where $r_0 = e^2/(4\pi\epsilon_0 mc^2)$ is the classical radius of the particle (with charge e and mass m), N_b is the bunch population, γ_0 is the relativistic factor for the beam, and $\Gamma = (2\pi)^3 \epsilon_{nx} \epsilon_{ny} \epsilon_{nz}$ is the phase space volume of a bunch with (normalised) emittances ϵ_{nx} , ϵ_{ny} , ϵ_{nz} .

The parameters \tilde{a} , \tilde{b} , \tilde{q} are defined:

$$\tilde{a} = \frac{\sigma_h}{\gamma_0} \sqrt{\frac{\beta_x}{\epsilon_x}}, \quad \tilde{b} = \frac{\sigma_h}{\gamma_0} \sqrt{\frac{\beta_y}{\epsilon_y}}, \quad \tilde{q} = \beta_0 \sigma_h \sqrt{\frac{2b_{\max}}{r_0}}, \quad (22)$$

where:

$$\frac{1}{\sigma_h^2} = \frac{1}{\sigma_\delta^2} + \frac{\eta_x^2}{\beta_x \epsilon_x} + \frac{\eta_y^2}{\beta_y \epsilon_y}, \quad (23)$$

σ_z and σ_δ are the bunch length and energy spread, β_x , β_y are the horizontal and vertical beta functions, η_x , η_y are the horizontal and vertical dispersion, and b_{\max} is the maximum impact parameter in a scattering event, with the impact parameter defined as shown in Fig. 5. The ‘‘Piwinski function’’ $f(\tilde{a}, \tilde{b}, \tilde{q})$, shown for selected values of the parameters in Fig. 6, is given by:

$$f(\tilde{a}, \tilde{b}, \tilde{q}) = 8\pi \int_0^1 \left(2 \ln \left(\frac{\tilde{q}}{2} \left(\frac{1}{\tilde{P}} + \frac{1}{\tilde{Q}} \right) \right) - 0.577 \dots \right) \frac{1 - 3u^2}{\tilde{P}\tilde{Q}} du, \quad (24)$$

where:

$$\tilde{P}^2 = \tilde{a}^2 + (1 - \tilde{a}^2)u^2, \quad \tilde{Q}^2 = \tilde{b}^2 + (1 - \tilde{b}^2)u^2. \quad (25)$$

The parameters \tilde{a} and \tilde{b} characterise the dependence of the scattering rate on the horizontal and vertical beta functions (respectively); but also include effects of coupling between transverse and longitudinal motion through σ_h and the dispersion functions. The dependence of the transverse growth rates on the dispersion arises from the fact that, because the closed orbit in a storage ring depends on the energy of the particle, a sudden change in the energy of a particle will lead to a change in betatron amplitude. The effect is analogous to quantum excitation in electron storage rings: a particle that emits a photon (in a dipole or insertion device) at a location of non-zero dispersion will undergo a change in betatron amplitude as a result of the change in closed orbit related to the change in energy of the particle.

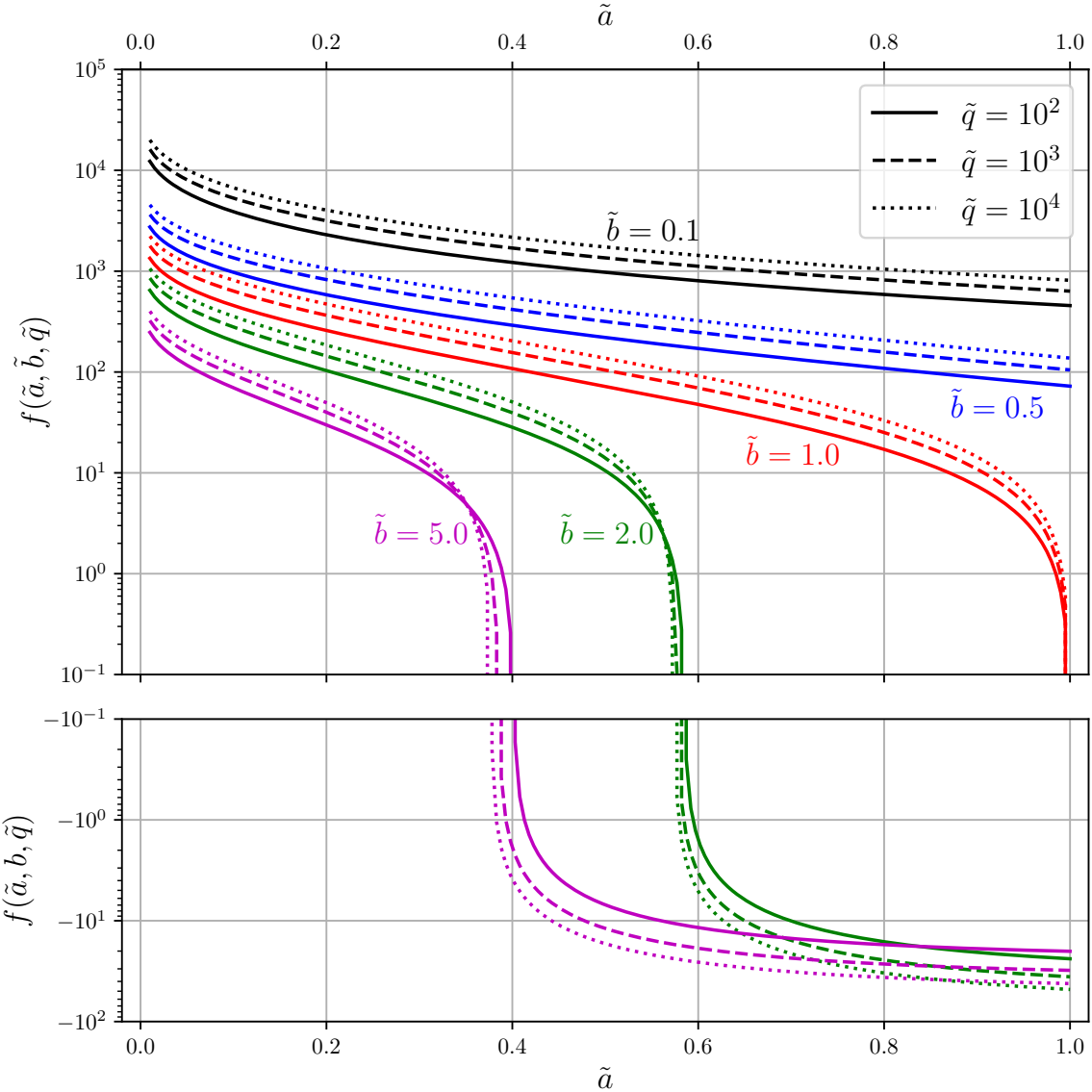


Fig. 6: Piwinski function f , defined by Eq. (24). The Piwinski function characterises the dependence of the growth rates on the beam properties, as expressed in Eqs. (18), (19) and (20). The parameters \tilde{a} and \tilde{b} , defined in Eq. (22), characterise (broadly) the dependence of the IBS scattering rate on the horizontal and vertical beta functions (respectively). The parameter \tilde{q} includes the dependence on the ratio of the maximum to minimum impact parameter in any collision between particles. Note the strong dependence of the Piwinski function on \tilde{a} and \tilde{b} , and the relatively weak dependence on \tilde{q} .

One of the difficulties in deriving formulae for the emittance growth rates resulting from IBS is the fact that the scattering amplitude in Eq. (15) diverges when the change q in the four-momentum of a particle involved in a collision is such that $q^2 = 0$. This occurs when there is no change in energy of either particle in the collision, which can happen in two cases: first, where the particles collide head-on (impact parameter equal to zero), and second, in the limit of large impact parameter. To avoid divergence of the formulae for the growth rates, it is necessary to set upper and lower limits on the impact parameter. Unfortunately, there is no completely rigorous way of specifying the limits given the model on which the theory is based. For example, if the impact parameter is very large, then this implies that

at least one of the particles is a large distance from the core of the bunch: in a Gaussian distribution, although the density of particles falls with increasing distance from the centre, mathematically it never falls completely to zero. The reduction in particle density with increasing impact parameter balances the divergence of the scattering amplitude to some extent, but is not sufficient on its own to prevent divergence of the formulae for the emittance growth rates.

To address the issues associated with the divergence of the scattering amplitude, it is usual to take a pragmatic approach and set upper and lower limits on the impact parameter that reflect the nature of the particles and the distribution of particles in a bunch. Conventionally, the lower limit is specified to be the classical radius of the particle, $r_0 = e^2/(4\pi\epsilon_0 mc^2)$, where e is the charge on the particle and m is the mass. The upper limit is taken to be the smallest dimension of the bunch: this is usually the vertical beam size, so that $b_{\max} = \sqrt{\beta_y \epsilon_y}$ in Eq. (22). Although these choices may seem rather arbitrary, fortunately the scattering rates are fairly insensitive to the precise values chosen: the limits enter the formulae for the scattering rates as a ratio in the expression for the parameter \tilde{q} in Eq. (22), and we see from Fig. 6 that the Piwinski function $f(\tilde{a}, \tilde{b}, \tilde{q})$ has a relatively weak dependence on \tilde{q} (compared to its dependence on \tilde{a} and \tilde{b}).

3.3 Derivatives of the lattice functions: Martini's formulae

Piwinski's formulae for the IBS growth rates are expressed in terms of the lattice functions (beta function and dispersion). In principle, it is possible to take into account variations in the lattice functions around a storage ring by calculating the growth rates as a function of position. However, Piwinski's formulae neglect effects associated with the derivatives of the lattice functions with respect to position, i.e. dependence of the scattering rates on $\beta'_{x,y} = -2\alpha_{x,y}$ and η'_x . These quantities describe (respectively) the correlation between the transverse coordinates and momenta of particles, and the dependence of the transverse momentum of a particle following a closed orbit on the energy of the particle. Since the rate of momentum transfer between particles in IBS depends on the distributions of particles in phase space ($\rho(x, p)$ in Eq. (14)), the values of the derivatives of the lattice functions can affect the emittance growth rates. Piwinski's theory was generalised by Martini [10] to take the derivatives of the lattice functions into account. The corrections are generally quite small; we do not give the formulae here, but refer the reader to the literature, e.g. [10–12].

3.4 Bjorken–Mtingwa formulae

Working independently from Piwinski, and following an alternative approach to the analysis, Bjorken and Mtingwa [13] derived expressions for the IBS growth rates that take a different form from the formulae given in the previous section. In the Bjorken–Mtingwa formalism, the growth rates are given by:

$$\frac{1}{T_i} = 4\pi A(\log)_{\text{BM}} \times \left\langle \int_0^\infty d\lambda \sqrt{\frac{\lambda}{\det(L + \lambda I)}} \left[\text{Tr}(L_i) \text{Tr}\left(\frac{1}{L + \lambda I}\right) - 3 \text{Tr}\left(\frac{L_i}{L + \lambda I}\right) \right] \right\rangle_C,$$

where A is given by Eq. (21), I is the identity matrix, the matrices L_i are given by:

$$L_x = \frac{\gamma_0 \sqrt{\beta_x \mathcal{H}_x}}{\epsilon_x} \begin{pmatrix} \frac{1}{\gamma_0} \sqrt{\frac{\beta_x}{\mathcal{H}_x}} & \sin(\varphi_x) & 0 \\ \sin(\varphi_x) & \gamma_0 \sqrt{\frac{\mathcal{H}_x}{\beta_x}} & 0 \\ 0 & 0 & 0 \end{pmatrix}, \quad (26)$$

$$L_y = \frac{\gamma_0 \sqrt{\beta_y \mathcal{H}_y}}{\epsilon_y} \begin{pmatrix} 0 & 0 & 0 \\ 0 & \gamma_0 \sqrt{\frac{\mathcal{H}_y}{\beta_y}} & \sin(\varphi_y) \\ 0 & \sin(\varphi_y) & \frac{1}{\gamma_0} \sqrt{\frac{\beta_y}{\mathcal{H}_y}} \end{pmatrix}, \quad (27)$$

$$L_z = \frac{\gamma_0^2}{\sigma_\delta^2} \begin{pmatrix} 0 & 0 & 0 \\ 0 & 1 & 0 \\ 0 & 0 & 0 \end{pmatrix}, \quad (28)$$

and L is defined as:

$$L = L_x + L_y + L_z. \quad (29)$$

\mathcal{H}_x and \mathcal{H}_y are the horizontal and vertical dispersion invariants⁵, defined in terms of the Twiss parameters and the dispersion functions. The horizontal dispersion invariant is given by:

$$\mathcal{H}_x = \gamma_x \eta_x^2 + 2\alpha_x \eta_x \eta_{px} + \beta_x \eta_{px}^2. \quad (30)$$

A similar expression holds for the vertical dispersion invariant \mathcal{H}_y . The function φ_x is defined by:

$$\tan(\varphi_x) = -\beta_x \frac{\eta_{px}}{\eta_x} - \alpha_x, \quad (31)$$

with a similar definition for φ_y . The quantities \mathcal{H}_x and ϕ_x , with their counterparts in the vertical direction, describe the amplitude and phase of the dispersion at different points around a storage ring. In particular, the horizontal dispersion at any point in the ring can be written:

$$\eta_x = \sqrt{\beta_x \mathcal{H}_x} \cos(\varphi_x), \quad (32)$$

$$\eta_{px} = -\sqrt{\frac{\mathcal{H}_x}{\beta_x}} (\sin(\varphi_x) + \alpha_x \cos(\varphi_x)). \quad (33)$$

In this respect, the functions \mathcal{H}_x and ϕ_x are analogous to the betatron action and phase that describe betatron oscillations of particles moving around the ring.

The quantity $(\log)_{\text{BM}}$, sometimes known as the *Coulomb log* is defined as:

$$(\log)_{\text{BM}} = \ln\left(\frac{b_{\text{max}}}{b_{\text{min}}}\right), \quad (34)$$

where b_{max} is the maximum impact parameter that can occur in the collision between two particles in the beam, and b_{min} is the minimum impact parameter that can occur. The values for these parameters are sometimes chosen as follows:

$$b_{\text{max}} = \min(\sigma_x, \sigma_y), \quad (35)$$

$$b_{\text{min}} = r_0, \quad (36)$$

where $\min(\sigma_x, \sigma_y)$ is the smaller of the horizontal and vertical beam size, and r_0 is the classical radius of the particles.

The expressions for the IBS growth rates in the Bjorken–Mtingwa formula (26) take a form that looks very different from the expressions for the growth rates in the Piwinski formulae (18), (19) and (20). However, Bane [14] has shown that, with certain assumptions, the Piwinski formulae and the Bjorken–Mtingwa formulae are in good agreement with each other. This is discussed further in the following section, where we consider approximations to the formulae for the IBS growth rates that simplify the computations of the growth rates for high energy beams.

⁵The functions \mathcal{H}_x and \mathcal{H}_y are referred to as “invariants” because outside of dipole magnets they take constant values as functions of position along a beamline.

3.5 High energy approximations

The complexities of the formulae developed by Piwinski and by Bjorken and Mttingwa for the IBS growth rates have motivated efforts to find simplified expressions, to allow faster and more convenient computation of the growth rates. Computational efficiency is important when calculating how the emittance in a storage ring changes over time: the IBS growth rates depend on the beam emittance, so as the emittance changes, the growth rates must be recalculated. In electron storage rings the equilibrium emittance is determined by the balance between synchrotron radiation damping and emittance growth from quantum excitation and IBS; since the IBS growth rates depend on the emittance, some iteration is needed to find the value of the emittance for which all the effects balance. Computational efficiency is again a consideration in performing the calculations.

An important step in reducing the time needed to calculate the IBS growth rates is the replacement of the integral in Eq. (24) that appears in Piwinski's formulae with a function that can be more rapidly evaluated. There are various approximations that may be made to this function; here, we mention the high-energy approximation derived by Bane [14] and a later high-energy approximation derived by Mttingwa et al. [16].

Bane started from the Bjorken–Mttingwa formulae to find formulae for the IBS growth rates that can be written as follows:

$$\frac{1}{T_z} \approx \frac{r_0^2 c N(\log)}{16\gamma^3 \varepsilon_x^{3/4} \varepsilon_y^{3/4} \sigma_z \sigma_\delta^3} \langle \sigma_H g_{\text{Bane}}(a/b) (\beta_x \beta_y)^{-1/4} \rangle, \quad (37)$$

$$\frac{1}{T_{x,y}} \approx \frac{\sigma_\delta^2 \langle \mathcal{H}_{x,y} \rangle}{\varepsilon_{x,y}} \frac{1}{T_z}, \quad (38)$$

where:

$$a = \frac{\sigma_H}{\gamma} \sqrt{\frac{\beta_x}{\varepsilon_x}}, \quad b = \frac{\sigma_H}{\gamma} \sqrt{\frac{\beta_y}{\varepsilon_y}}, \quad \frac{1}{\sigma_H^2} = \frac{1}{\sigma_\delta^2} + \frac{\mathcal{H}_x}{\varepsilon_x} + \frac{\mathcal{H}_y}{\varepsilon_y}, \quad (39)$$

and the function g_{Bane} is given by:

$$g_{\text{Bane}}(\alpha) = \frac{2\sqrt{\alpha}}{\pi} \int_0^\infty \frac{du}{\sqrt{1+u^2} \sqrt{\alpha^2+u^2}}. \quad (40)$$

A numerical fit to $g_{\text{Bane}}(\alpha)$ leads to the approximation:

$$g_{\text{Bane}}(\alpha) \approx \alpha^{(0.021 - 0.044 \ln(\alpha))}. \quad (41)$$

Bane's formulae are valid for $a, b \ll 1$ (which will be the case if the beam is cooler longitudinally than transversely), and if effects from the gradients of the lattice functions (dispersion and beta functions) are negligible.

Alternative expressions for the (approximate) IBS growth rates, again avoiding the integral in Piwinski's formulae, were obtained by Mttingwa et al. [16] using an earlier approximation for the function $f(a, b, q)$ by Mttingwa and Tollestrup [15]:

$$f(a, b, q) \approx -\frac{4\pi^{3/2}}{a} g(b) \ln(q), \quad (42)$$

where $g(b)$ is given by:

$$g(b) = \sqrt{\frac{\pi}{b}} \left(P_{-1/2}^0(\theta) + \text{sgn}(b-1) \frac{3}{2} P_{-1/2}^{-1}(\theta) \right). \quad (43)$$

In this expression, $\theta = (b^2 + 1)/2b$, and $P_\nu^\mu(\theta)$ are associated Legendre functions. Unfortunately, the functions $P_\nu^\mu(\theta)$ are not easy to evaluate, and this can further limit the advantages of the approximation (see Eq. (42)) compared to the use of the full expression (see Eq. (24)) involving an integral.

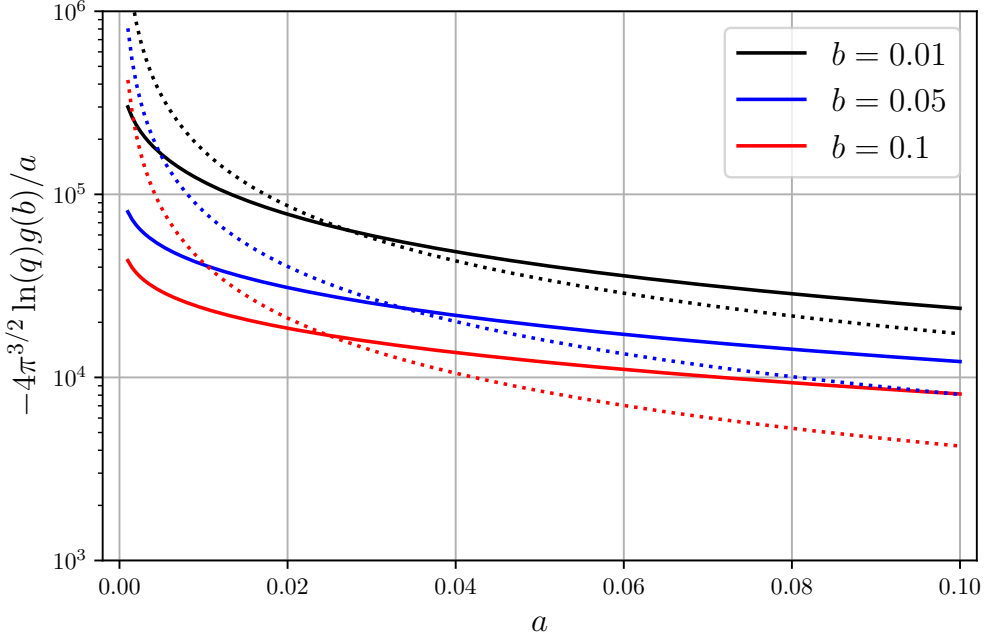


Fig. 7: Piwinski function f (solid lines) compared with the high-energy approximation (42) (dotted lines). In this case, $q = 10^3$. The Piwinski function is shown in more detail (and over a larger range of parameters) in Fig. 6.

However, use of Eq. (42) leads to the ‘‘completely integrated modified Piwinski’’ (CIMP) formulae for the IBS growth rates:

$$\frac{1}{\tau_x} \approx 2\pi^{\frac{3}{2}} A \left\langle -a \ln\left(\frac{q^2}{a^2}\right) g\left(\frac{b}{a}\right) + \frac{\mathcal{H}_x \sigma_H^2}{\epsilon_x} G(a, b, q) \right\rangle \quad (44)$$

$$\frac{1}{\tau_y} \approx 2\pi^{\frac{3}{2}} A \left\langle -b \ln\left(\frac{q^2}{b^2}\right) g\left(\frac{a}{b}\right) + \frac{\mathcal{H}_y \sigma_H^2}{\epsilon_y} G(a, b, q) \right\rangle \quad (45)$$

$$\frac{1}{\tau_z} \approx 2\pi^{\frac{3}{2}} A \left\langle \frac{\sigma_H^2}{\sigma_p^2} G(a, b, q) \right\rangle. \quad (46)$$

The function $G(a, b, q)$ is given by:

$$G(a, b, q) = \frac{\ln\left(\frac{q^2}{a^2}\right) g\left(\frac{b}{a}\right)}{a} + \frac{\ln\left(\frac{q^2}{b^2}\right) g\left(\frac{a}{b}\right)}{b}, \quad (47)$$

with:

$$a = \frac{\sigma_H}{\gamma_0} \sqrt{\frac{\beta_x}{\epsilon_x}}, \quad b = \frac{\sigma_H}{\gamma_0} \sqrt{\frac{\beta_y}{\epsilon_y}}, \quad q = \beta_0 \sigma_H \sqrt{\frac{2\beta_y \epsilon_y}{r_0}}, \quad (48)$$

and:

$$\frac{1}{\sigma_H^2} = \frac{1}{\sigma_\delta^2} + \frac{\mathcal{H}_x}{\epsilon_x} + \frac{\mathcal{H}_y}{\epsilon_y}. \quad (49)$$

The approximations leading to these results are again valid in the high energy regime, where a and b are much smaller than q . A comparison between the Piwinski function $f(a, b, q)$ and the approximation (42) is shown in Fig. 7. For a numerical comparison of the IBS growth rates calculated using the full Piwinski formulae, Bane’s approximation and the CIMP approximation in a particular case, see [16].

4 Tests of IBS theory against experimental measurements

Although the effects of intrabeam scattering have long been observed and there has been extensive work on understanding the theory and on developing mathematical models, validation of the formulae for the emittance growth rates has been difficult. There are two main reasons for this. First, although emittance growth from IBS can be significant, the effects of IBS are often weak relative to other phenomena that may lead to changes in emittance (such as space charge effects, nonlinear behaviour resulting from higher-order multipole components in the magnets, or wakefield effects). Separating IBS emittance growth from growth caused by other effects is not straightforward. Secondly, the IBS emittance growth depends on many beam and lattice properties: without a full and detailed knowledge of all the relevant quantities the IBS emittance growth can only be calculated from the theory by making some assumptions, and this inevitably leads to some uncertainty in the results.

Despite the challenges in testing the theoretical models of IBS, quantitative studies have been carried out over the years in a variety of machines, covering a wide range of parameter regimes. Here, we mention briefly a few of those studies.

4.1 KEK-ATF

The Accelerator Test Facility (ATF) at KEK was developed to support research for damping rings for a future linear collider. It operates as a low-emittance storage ring with full-energy injection at 1.28 GeV. A suite of diagnostics provide detailed information about the beam properties, including energy spread and emittance. A particular goal was the demonstration of vertical emittance of a few picometres. In 2002, a detailed study was carried out to characterise the damping of the beam emittances after injection. It was found that initially the emittances reduced at the rate expected from synchrotron radiation effects, but that the longitudinal emittance, rather than damping monotonically to an equilibrium value (as would be expected from radiation damping), passed through a minimum about 100 ms after beam injection, before increasing to a final equilibrium that depended on the bunch charge. This behaviour can be seen in the results shown in Fig. 8.

The fact that the longitudinal emittance passes through a minimum following injection (before reaching some equilibrium value above the minimum) can be understood by considering the effects of IBS. In an electron storage ring, the radiation damping time in the longitudinal direction is usually about half the transverse damping time: this means that the longitudinal emittance can approach an equilibrium value much sooner than the transverse emittances. In the case of the ATF, IBS effects are negligible in an injected bunch with large emittances, and become significant only when the transverse emittances reach low values. A vertical emittance of a few picometres leads to IBS emittance growth rates that are comparable with the radiation damping rates. As a result, once the vertical emittance approaches its equilibrium value (between 50 ms and 100 ms after injection into the ATF storage ring) IBS effects become strong enough to increase the longitudinal emittance. The final longitudinal and transverse emittance values depend on the bunch charge, which is readily controlled in the ATF.

The plot in Fig. 8 [17] shows a comparison between measurements (points with circular, triangular or square markers on the plot, according to the bunch charge) and calculations based on the Bjorken–Mtingwa formalism [18]. Although the agreement is not perfect, the behaviour of the longitudinal emittance is described well using the theory.

4.2 CELSIUS

The CELSIUS storage ring [19] operated between 1989 and 2005 at the Svedberg Laboratory, Uppsala University, and was part of an accelerator facility for research into nuclear physics. The storage ring was designed to cool and accelerate beams covering a range of species and energies, from protons (up to 1360 MeV kinetic energy) to ions with $A \sim 100$ (470 MeV per nucleon for particles with charge to mass ratio 1/2). Especially at the lower end of the energy range, intrabeam scattering effects could be

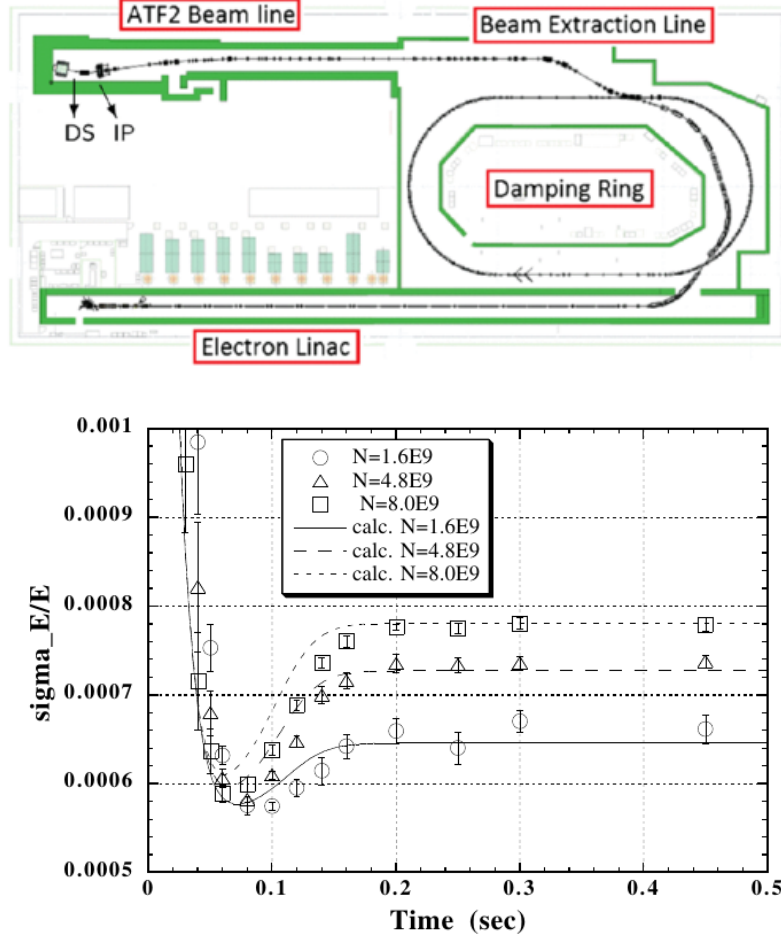


Fig. 8: Top: layout of the KEK Accelerator Test Facility (ATF), showing the 1.28 GeV electron linac, the storage (or damping) ring, and the extraction line. Bunches can be extracted from the ring at any time following injection; high dispersion in the extraction line allow accurate measurements of beam energy spread to be made. Bottom: evolution of the energy spread of bunches following injection into the ATF. Three different bunch populations (1.6×10^9 for circular markers, 4.8×10^9 for triangular markers and 8.0×10^9 for square markers) are shown. Markers show experimental data; lines show theoretical expectations, taking into account synchrotron radiation damping and intrabeam scattering. Because the longitudinal damping time is shorter than the transverse damping times, the energy spread reaches a very low value while the vertical emittance is still relatively large; as the vertical emittance continues to damp, the IBS growth rates increase leading to an increase in the energy spread.

significant. In normal operation, the beam emittances were damped by electron cooling; but the ability to turn off the cooling provided the ability to make measurements of IBS emittance growth in a range of different parameter regimes.

Some results from emittance measurements at CELSIUS are shown in Fig. 9 [8]. Each plot shows a comparison between measurements of the horizontal emittance as a function of time after switching off the beam cooling and the predictions from IBS theory under the corresponding conditions. Results are shown for 48 MeV protons, 400 MeV protons, and 200 MeV/u N^{7+} ions, with two different bunch populations in each case. Measurements were made with the storage ring operating above the transition energy. Theoretical predictions, made using Martini's formulae and on the formulae of Bjorken and Mtingwa, are in good agreement with the measurements. It should be noted, however, that only the horizontal emittance was measured: for the calculations, the bunch length and energy spread were assumed

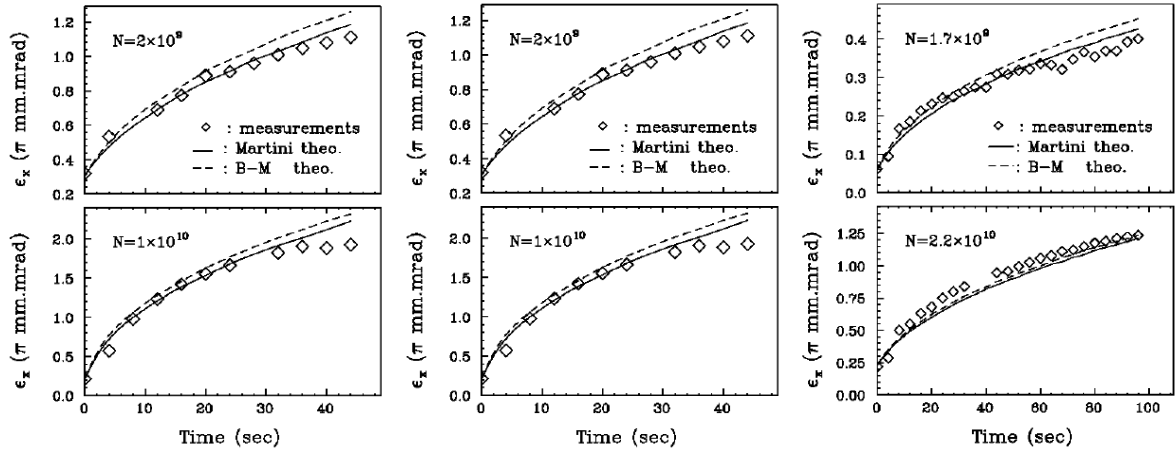


Fig. 9: Measurements of intrabeam scattering in the CELSIUS storage ring [8]. Each plot shows the horizontal emittance as a function of time after turning off the transverse beam cooling. Measurements (diamond-shaped markers) are compared with calculations based on the formulae of Martini (solid lines) and Bjorken–Mtingwa (dashed lines). Left: 48 MeV proton beam with bunch populations 2×10^9 (top) and 1×10^{10} (bottom). Middle: 400 MeV proton beam with bunch populations 1.7×10^9 (top) and 2.2×10^{10} (bottom). Right: 200 MeV/u beam of N^7+ ions with bunch populations 8.3×10^8 (top) and 1.7×10^9 (bottom).

to be equal to nominal values based on values measured for injected bunches and reduced according to the expected effects of the beam cooling. The vertical emittance was assumed to be equal to the horizontal emittance. For further details, the reader is referred to [8].

4.3 Gold Ions in RHIC

The measurements of IBS emittance growth in CELSIUS shown in Section 4.2 were made with the storage ring operating above transition. Measurements of the effects of IBS on the emittances of beams in a storage ring below transition have also been made, for example in the Relativistic Heavy Ion Collider (RHIC) at Brookhaven [20]. IBS was of particular concern in RHIC because of the fact that ion beams were generally injected at low energy, below transition in the storage ring, before the energy was ramped to the full energy required for collider operation; acceleration involved crossing the transition energy (with associated manipulations of the longitudinal phase space) and any increase in longitudinal emittance of the beams after injection could lead to particle loss at transition crossing.

In 2000, a set of experiments was performed using gold ions. Measurements of bunch length and transverse (vertical) beam size were made over a period of half an hour following beam injection, with the ions having a relativistic factor $\gamma = 10.25$. Bunch length measurements were made using a wall current monitor, which gave the charge density as a function of time with a resolution of 0.25 ns; typical results are shown in Fig. 10, left. Transverse beam size measurements were made using ionization beam profile monitors [21]. Because of technical issues at the time of the measurements, only the vertical beam size was measured; to compare the results of measurements with simulations, it was assumed that the horizontal beam size was equal to the vertical beam size. Simulations were performed with two different computer codes, both making high-energy approximations to the IBS growth rate formulae [22, 23]. A comparison between measurements and simulations of the growth in the bunch length is shown for five different cases in Fig. 10, right.

In most cases, there is reasonable agreement between the measured growth rates and the growth rates predicted by the computer codes. In the case showing a significant difference (with a measured growth rate about twice the growth rate predicted by the computer codes) it is thought that some mecha-

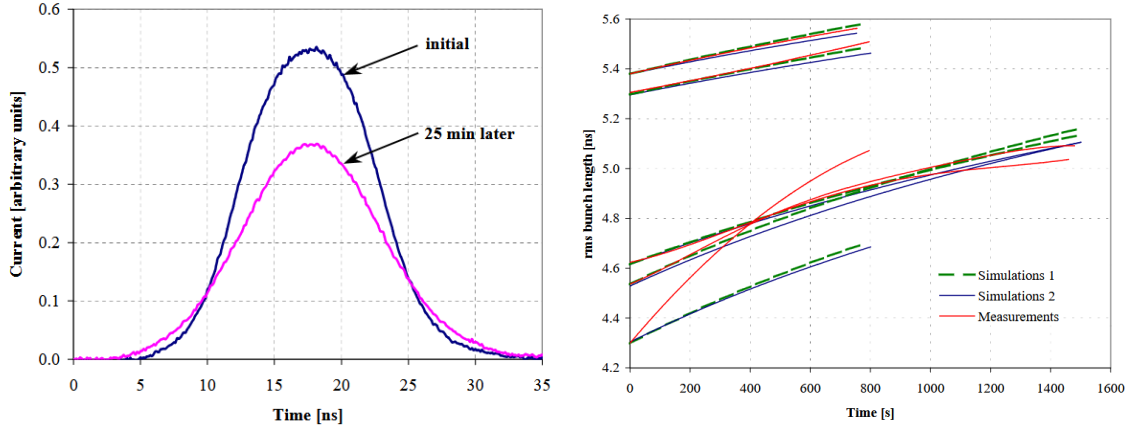


Fig. 10: Measurements of intrabeam scattering in beams of gold ions in RHIC at injection energy (relativistic $\gamma = 10.25$) [20]. At injection, the ring is operating below transition. Left: longitudinal charge profile immediately after injection (blue line) and after 25 minutes (magenta line). Right: increase of bunch length with time for five different sets of measurements. Results from two different simulation codes (dashed green line and solid blue line) are compared with measurements (solid red line).

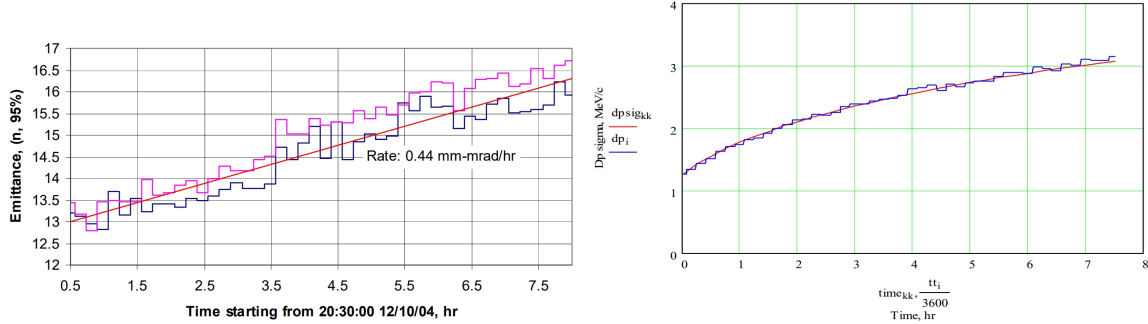
nism other than intrabeam scattering may have contributed to the growth in the bunch length.

In a ring operating below transition, the theory predicts that intrabeam scattering should lead to a redistribution of the emittances, with the sum of the emittances remaining bounded according to Eq. (10). Therefore, in the case of the measurements made in RHIC, with an increasing bunch length it is expected that there should be a fall in the transverse emittance. However, only one of the computer codes predicted a reduction in transverse emittance; for reasons that are not completely clear (but that may be to do with the use of a high energy approximation in the calculations) the other code predicted a slow growth in transverse emittance. The measurements also showed an increase in transverse emittance, though it should be remembered that only the vertical emittance was measured during the experiments. The reason for this behaviour is again not clear, though it is again possible that effects other than intrabeam scattering were contributing to the emittance growth.

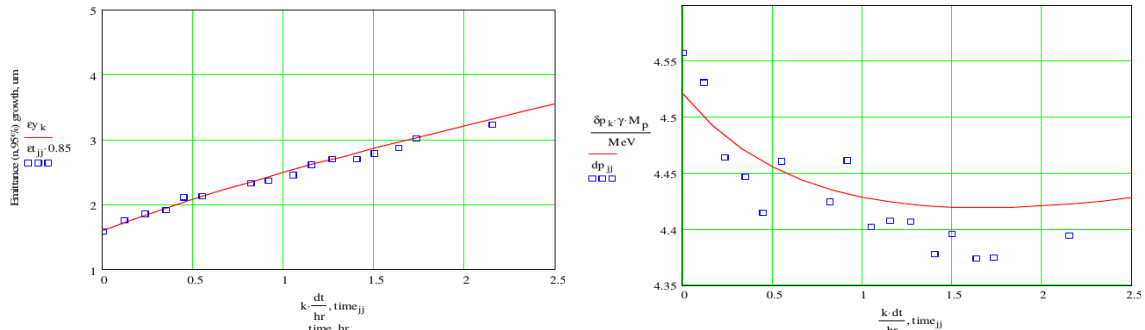
4.4 Protons in the Fermilab Recycler ring

Measurements of IBS emittance growth in a storage ring below transition were also made using the Fermilab Recycler, a proton/antiproton storage ring operating at a fixed beam momentum of 9.8 GeV/c. The beam momentum at transition is 19.4 GeV/c. In preparation for the Run II luminosity upgrade of the Tevatron, experiments were carried out to characterise the effects of IBS on the longitudinal and transverse emittances of beams in the Recycler ring: results are reported in Ref. [24]. The momentum spread was of particular interest because of the need to produce beams with a small longitudinal emittance in the Tevatron. Measurements in the Recycler were first performed with a very low initial momentum spread (leading to longitudinal heating) and then with a larger initial momentum spread (resulting in longitudinal cooling). Some results are shown in Fig. 11.

The upper two plots in Fig. 11 show the results of measurements with a bunch of 100×10^{10} protons, with transverse emittance measurements in the left-hand plot, and energy spread measurements on the right. In this case, the initial energy spread is small and IBS leads to an increase in the longitudinal emittance. With the ring below transition, it is then expected that there will be some cooling in the transverse emittance. The measurements actually show a growth over time in the transverse emittance, at a rate of 0.44π mm mrad/hr; but this is a lower rate of growth than is measured under similar conditions but with a bunch population of 1×10^{10} . With the lower bunch charge, a transverse emittance growth rate of



(a) Proton bunch population 100×10^{10} .



(b) Antiproton bunch population 25×10^{10} .

Fig. 11: Measurements of intrabeam scattering in the Fermilab Recycler at 9.8 GeV/c beam momentum (below transition) [24]. Top: transverse emittance (left) and momentum spread (right) as functions of time in a bunch of 100×10^{10} protons. With an initially low energy spread, IBS leads to an increase in longitudinal emittance. The transverse emittance also increases, but at a slower rate than would be expected from gas scattering under the relevant conditions. Bottom: transverse emittance (left) and momentum spread (right) as functions of time in a bunch of 25×10^{10} antiprotons. In this case, the initial longitudinal emittance (right) is relatively large, and reduces over time from the effects of IBS. The growth rate of the transverse emittance (left) is increased in this case above the rate expected from gas scattering.

0.60 π mm mrad/hr is observed: with this bunch population effects of intrabeam scattering are negligible, and the transverse emittance growth is the result of scattering between particles in the bunch and residual gas in the vacuum chamber. The emittance growth from gas scattering is independent of bunch charge: intrabeam scattering in this case, therefore, leads to a cooling of the transverse emittance as expected from the theory.

The lower two plots in Fig. 11 show the results of measurements with a bunch of 25×10^{10} antiprotons, with transverse emittance in the left-hand plot and momentum spread in the right-hand plot. In this case, the initial momentum spread is much larger than in the previous case (100×10^{10} protons per bunch), and IBS leads to longitudinal cooling. The red line in the left hand plot in Fig. 11 (b) shows the predicted emittance growth from IBS and gas scattering. The growth rate from gas scattering is the only free parameter in the fit: the best fit is obtained with a gas scattering growth rate of 0.60π mm mrad/hr, which is consistent with separate measurements (at low bunch population). With IBS, the growth rate is close to 0.9π mm mrad/hr, so IBS makes a positive contribution to the transverse emittance growth. Again, this is consistent with the theory which predicts transverse heating under conditions where there is longitudinal cooling.

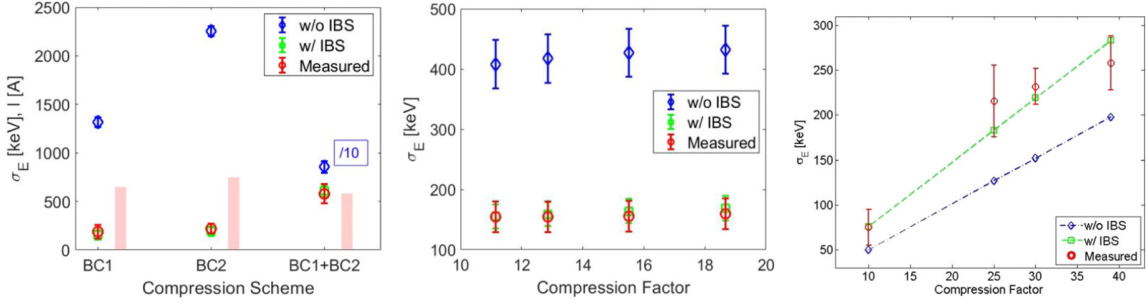


Fig. 12: Observations of intrabeam scattering in the FERMI FEL driver with electron bunches accelerated to energy between 713 MeV and 754 MeV [6]. Left: without use of a laser heater to suppress coherent synchrotron radiation (CSR) by increasing the energy spread, the measured energy spread (red markers) with each of three bunch compression schemes is significantly below the energy spread that would be expected in the absence of IBS (blue markers). Including IBS in the simulations leads to energy spreads in good agreement with measurement: the increase in energy spread at low energy from IBS suppresses the effects of CSR that can lead to much larger increases in energy spread. Middle: energy spread as a function of compression factor in BC1, with bunch charge 650 pC and with laser heater turned off. The energy spread is dominated by CSR so does not increase with the compression factor; but the impact of CSR is reduced by the increase in energy spread caused by IBS. Right: energy spread as a function of compression factor in BC1, with bunch charge 100 pC and with laser heater turned on. In this case, the laser heater almost entirely suppresses the effects of CSR so the energy spread increases with compression factor as expected; an increase in energy spread from IBS can now also be observed.

4.5 The FERMI Free-Electron Laser

Observations of IBS effects have also been made in the driver for the FERMI free-electron laser [6], in a very different parameter regime from those in the machines mentioned so far. Like the KEK-ATF, the FERMI FEL is an electron accelerator; but whereas the KEK-ATF is a storage ring the FERMI FEL is a single-pass beamline. With improvements in technology in recent years, FEL injector systems have become capable of producing electron bunches with charge densities high enough for IBS effects to be significant on the short timescales associated with single-pass machines.

For a short-wavelength (VUV or X-ray) FEL to operate effectively, it is important to achieve a short bunch length and low energy spread in the electron bunch reaching the undulator. Considerable efforts are made to understand and control both the bunch length and the energy spread, and detailed models including all relevant physical effects are needed if an accurate match between simulations and measurements is to be achieved. The FERMI FEL, like other short-wavelength free-electron lasers, relies on bunch compressors to reduce the bunch length to the range required for FEL operation. Bunch compressors work by rotating the longitudinal phase space, and necessarily lead to an increase in energy spread: in the absence of collective effects, the energy spread increases by the same factor by which the bunch length is reduced, so that the longitudinal emittance (essentially, the product of the bunch length and the energy spread) is conserved. However, with high charge and short bunches, emission of coherent synchrotron radiation (CSR) in the dipoles in a bunch compressor can act back on particles in the bunch, leading to an increase in the energy spread far beyond the limit needed for FEL operation. The effect of CSR may be reduced by Landau damping: artificially increasing the energy spread (e.g. by interacting the bunch with a laser pulse in a ‘laser heater’) disrupts the coherent motion of the particles and suppresses emission of CSR. Although use of a laser heater leads to some increase in the energy spread, the increase can be significantly less than that resulting from CSR in the absence of a laser heater.

Figure 12 shows a comparison between energy spread measurements at the end of the FERMI linac (beam energy between 713 and 754 MeV with 100 pC bunch charge, or 900 MeV with 650 pC bunch charge) and the results of simulations. The left-hand plot shows the case of a 100 pC bunch, with

laser heater turned off; results for three different compression schemes are shown. Without IBS (blue points) simulations predict energy spread above 1200 keV: this is in large part due to CSR. Note that for the case of the combined bunch compression scheme (BC1+BC2) the point shown on the plot has been reduced by a factor of 10 to fit on the same axis as the other cases. If IBS effects are included, there is an effective suppression of CSR, and the results of the simulations are in good agreement with the measurements.

The central plot in Fig. 12 shows results for the case of a 650 pC bunch, again with the laser heater turned off. In this case, only the first bunch compressor (BC1) is used, but with a range of different compression factors. Without IBS, CSR is again expected to make a dominant contribution to the final energy spread; including IBS in the simulations shows that the consequent modest increase in energy spread is sufficient to suppress CSR to a significant degree. The results of simulations including IBS are in good agreement with the energy spread measurements.

Finally, the right-hand plot in Fig. 12 shows the energy spread in the case of a 100 pC bunch with the laser heater turned on, for different compression factors in BC1. The laser heater suppresses CSR almost entirely: in this case, we see the expected increase in energy spread with increasing compression factor. Under these conditions, IBS no longer has a beneficial effect in suppressing CSR (which has already been largely eliminated by the laser heater) but instead makes a positive contribution to the energy spread. The measured energy spread is larger than expected from simulations in which IBS is omitted; however, although the agreement is not perfect, the simulations are consistent with the measurement results if IBS is included.

5 Final remarks

Intrabeam scattering has continued to be much studied since the initial observations and theoretical investigations in the 1960's and 1970's. Even though the fundamental processes are well understood, predicting the effects of IBS in specific cases remains difficult because of the complexity of the calculations. Experimental studies are challenging because of the difficulty in making precise measurements of all the relevant parameters, and also because other effects can lead to changes in emittance on the timescale of the changes that would be expected from IBS.

Historically, IBS has been of greater significance in hadron accelerators than in electron machines. This is because IBS effects have generally been too slow to have much impact in single-pass systems; and in storage rings, radiation damping in the case of electrons dominates over emittance growth from IBS. In recent years, however, electron storage rings have started to operate in regimes where emittance growth rates from IBS have an impact on the equilibrium beam properties – this is particularly the case for the latest generation of synchrotron light sources, operating with ultra-low emittances (of the order of tens of picometres). IBS effects have now even been observed in electron beams in a single-pass system, namely the driver for the FERMI FEL. Meanwhile, experimental studies in hadron storage rings have been carried out over a wide range of conditions, including in proton, antiproton and ion beams, and in rings operating above and below transition. The overall picture that emerges is one that generally supports the validity of the IBS theories.

The first detailed theoretical treatment of IBS, by Piwinski in the early 1970's, continues to be widely used as the basis for computing emittance growth rates from IBS in many different parameter regimes, albeit with some extensions to include aspects omitted in the original treatment (such as the variation of beta functions around the circumference of a storage ring). The theory of Bjorken and Mtingwa, published in the early 1980's, provides an alternative formalism. Other researchers have contributed in attempting to provide approximations that can be used in certain regimes (notably, at high energy) to simplify the calculations and speed up the computations. Despite dramatic improvements in computing power over the years, work to develop formulae allowing rapid, accurate computation of IBS growth rates seems likely to continue.

Understanding IBS has been important for the design and operation of many different accelerators. The push to parameter regimes with ever-higher charge density (high bunch charge with low emittance and bunch length) seems likely to make IBS of increasing significance in future facilities, including hadron and electron storage rings, and even in single-pass machines such as free-electron lasers.

References

- [1] M. Ferrario, M. Migliorati and L. Palumbo, *Space charge effects*, in *Proceedings of the CERN Accelerator School: Advanced Accelerator Physics Course*, 18–29 August 2013, Trondheim, Norway, CERN-2014-009 (2014), pp. 331–356.
- [2] G. Franchetti, *Space charge in circular machines*, in *Proceedings of the CERN Accelerator School: Intensity Limitations in Particle Beams*, 2–11 November 2015, Geneva, Switzerland, CERN-2017-006-SP (2017), pp. 353–390.
- [3] C. Bernardini et al, *Lifetime and beam size in a storage ring*, Phys. Rev. Lett. **10**, 407 (1963), pp. 407–409.
- [4] A. Piwinski, *Intra-beam-scattering*, in *Proceedings of the 9th International Conference on High-Energy Accelerators (HEACC74)*, 2–7 May, 1974. Stanford, CA, USA (1974).
- [5] A. Piwinski, J.D. Bjorken and S.K. Mtingwa, *Wilson Prize article: Reflections on our experiences with developing the theory of intrabeam scattering*, Phys. Rev. Accel. Beams **21**, 114801 (2018).
- [6] S. Di Mitri et al, *Experimental evidence of intrabeam scattering in a free-electron laser driver*, New Journal of Physics, 22 (2020), 083053.
- [7] J. Gareyte, *The SPS $p\bar{p}$ collider*, in *Proceedings of the CERN Accelerator School: Antiprotons for Colliding-beam Facilities*, 1–10 September 1983, Geneva, Switzerland, CERN-SPS-84-3-DI-MST (1984), pp. 291–318.
- [8] Y.-N. Rao and L. Hermansson, *Intra-beam scattering at CELSIUS*, in *Proceedings of the 7th European Particle Accelerator Conference (EPAC2000)*, 26–30 June, Vienna, Austria (2000), pp. 1549–1551.
- [9] M.P. Ehrlichman et al, *Intrabeam scattering studies at the Cornell Electron Storage Ring Test Accelerator*, Phys. Rev. ST Accel. Beams **16**, 104401 (2013).
- [10] M. Martini, *Intrabeam scattering in the ACOL-AA machines*, Technical Report CERN PS/84-9 (AA) (1984).
- [11] M. Martini, *Intrabeam scattering: anatomy of the theory*, in *Proceedings of the CERN Accelerator School on Intensity Limitations in Particle Beams*, 2–11 November 2015, Geneva, Switzerland, CERN-2017-006-SP (2017), pp. 291–352.
- [12] M. Martini, F. Antoniou, Y. Papaphilippou, *Intrabeam scattering*, ICFA Beam Dynamics Newsletter 69 (2016), pp. 38–59.
- [13] J.D. Bjorken and S.K. Mtingwa, *Intrabeam scattering*, Particle Accelerators 13 (1983), pp. 115–143.
- [14] K. Bane, *A simplified model of intrabeam scattering*, in *Proceedings of the 8th European Particle Accelerator Conference (EPAC2002)*, 3–7 June 2002, Paris, France (2002), pp. 1443–1445.
- [15] S.K. Mtingwa and A.V. Tollestrup, *Intrabeam scattering formulae for asymptotic beams with unequal horizontal and vertical emittances*, Technical Report FERMILAB-Pub-89/224 (1987).
- [16] K. Kubo, S.K. Mtingwa and A. Wolski, *Intrabeam scattering formulas for high energy beams*, Phys. Rev. ST Accel. Beams **8**, 081001 (2005).
- [17] K. Kubo et al., *Extremely low vertical-emittance beam in the Accelerator Test Facility at KEK*, Physical Review Letters **88**, 19, 194801 (2002).
- [18] K. Kubo and K. Oide, *Intrabeam scattering in electron storage rings*, Phys. Rev. ST Accel. Beams **4**, 124401 (2001).

- [19] C. Ekström et al, *The CELSIUS project*, Phys. Scr. **1988**, 256 (1988).
- [20] W. Fischer et al, *Measurements of intra-beam scattering growth times with gold beam below transition in RHIC*, in *Proceedings of the 2001 Particle Accelerator Conference*, 18–22 June 2001, Chicago, IL, USA (2001), pp. 2857–2859.
- [21] P. Cameron et al, *The RHIC ionization beam profile monitor*, in *Proceedings of the 1999 Particle Accelerator Conference*, 29 March – 2 April 1999, New York, NY, USA (1999), pp. 2114–2116.
- [22] J. Wei, *Evolution of hadron beams under intrabeam scattering*, in *Proceedings of the 1993 Particle Accelerator Conference*, 17–20 May 1993, Washington DC, USA (1993), pp. 3651–3653.
- [23] G. Parzen, *Intrabeam scattering at high energies*, Nuclear Instruments and Methods in Physics Research Section A: Accelerators, Spectrometers, Detectors and Associated Equipment, Volume 256, Issue 2 (1987), pp. 231–240.
- [24] M. Hu and S. Nagaitsev, *Observation of longitudinal diffusion and cooling due to intrabeam scattering at the Fermilab Recycler Ring*, in *Proceedings of the 2005 Particle Accelerator Conference*, 16–20 May 2005, Knoxville, TN, USA (2005), pp. 1560–1562.